ORIGINAL RESEARCH ARTICLE

Effect of Solution Heat-Treatment on the Oxidation Resistance of Ni-Base Single-Crystal Superalloy

CHIHIRO TABATA, TOSHIO OSADA, TADAHARU YOKOKAWA, AYAKO IKEDA, KYOKO KAWAGISHI, and SHINSUKE SUZUKI

To clarify the effect of solution heat-treatment on the oxidation resistance of Ni-base single-crystal superalloy TMS-238, the evaluation of dendrite/inter-dendrite segregation of alloying elements in the as-cast and heat-treated samples, and its effect on cyclic oxidation resistance were investigated. Cyclic oxidation test results at 1100 °C for up to 150 cycles clearly showed that the as-cast samples with element segregations had lower oxidation resistance compared to heat-treated samples with homogeneous structure. Further, for the as-cast sample, rapid growth and spallation of oxide consisting of NiO, Cr_2O_3, and Al_2O_3 were observed around the dendrite core for 10 cycles of oxidation. Analysis of sub-surface on sample isothermally oxidized at 1100 °C for 10 minutes showed that rapid oxide growth is due to the formation of discontinuous Al_2O_3 layer at dendrite core with lower Al concentration. Furthermore, in this study, the threshold value of Al concentration and Gibbs energy for the formation of continuous Al_2O_3 layer were estimated and determined to be around 5.2 wt pct and -556.6 ± 0.5 kJ/mol, respectively. This indicated that the solution heat-treatment for TMS-238 should be conducted above 1305 °C for exhibiting oxidation resistance at 1100 °C, to meet the threshold value within the whole region between dendrite and inter-dendrite.

https://doi.org/10.1007/s11661-023-07205-7

I. INTRODUCTION

Ni-BASE single-crystal superalloys with γ/γ' two-phase structures are materials often used in the turbine blades for the hottest components in jet engines and gas turbines for power generation. To improve the thermal efficiency of the engines, the inlet gas temperatures are on the rise, and the turbine inlet temperature must be increased. The components must also be able to withstand the highest temperature and pressure within the engines. Therefore, the components often use single-crystal (SC) alloys.[1] To improve its high temperature creep strength and other mechanical properties, optimization of chemical compositions by alloy design,[2–5] as well as solution heat-treatment and aging heat-treatment temperatures[6–8] for Ni-base SC superalloys are being studied.

Solution heat-treatment of cast alloy is an important process for achieving a desired homogeneous γ/γ' two-phase structure,[9,10] since the as-cast materials have strong segregation of elements, leading to large differences in the compositions of the dendrite core and inter-dendrite[11,12] and observations of remaining eutectic phases. However, recent superalloys have significantly limited process windows for solution heat-treatment, and in order to avoid formations of eutectic phases, the heat-treatment process becomes severely complex.[6,13] On the other hand, alloys such as TMS-238, a 6th generation alloy with excellent creep strength, have larger process windows for heat-treatment.[14] But this material requires heat-treatment at temperatures as high as 1335 °C, and methods to reduce the process cost, such as decreasing the solution heat-treatment temperature and time, are needed.[11,14]

Furthermore, because Ni-base superalloys are often used at high temperatures, oxidation resistance becomes an important property as well. Therefore, measurement and observations of high temperature oxidation resistance of homogenized superalloys have been conducted,[15–21] and methods to predict the oxidation resistance of the

CHIHIRO TABATA, and KYOKO KAWAGISHI are with the National Institute for Materials Science (NIMS), 1-2-1 Sengen, Tsukuba, Ibaraki 305-0047, Japan and also with the Department of Materials Science, Waseda University, 3-4-1 Okubo, Shinjuku-ku, Tokyo 169-8555, Japan. Contact e-mail: chihiro448@akane.waseda.jp TOSHIO OSADA, TADAHARU YOKOKAWA, and AYAKO IKEDA are with the National Institute for Materials Science (NIMS). SHINSUKE SUZUKI is with the Department of Materials Science, Waseda University and with the Department of Applied Mechanics and Aerospace Engineering, Waseda University, 3-4-1 Okubo, Shinjuku-ku, Tokyo 169-8555, Japan and also with the Kagami Memorial Institute for Materials Science and Technology, Waseda University, Tokyo 169-0051, Japan.

Manuscript submitted June 21, 2023; accepted September 10, 2023. Article published online October 2, 2023

alloys at such temperatures[22] have been studied by various researchers. For example, Sato *et al.* proposed a method using effective valence index and Gibbs energy to predict whether the homogenized alloys will likely form α-Al_2O_3 for oxidation at 900 °C and 1000 °C.[23,24] Many also consider the effect of the composition of alloys on the oxidation resistance of alloys.[17,25–29] Hagen *et al.* reported on the difference in the scale width and cyclic oxidation at 850 °C and 1050 °C among the as-cast, short heat-treatment, and long heat-treatment on Co-base SC superalloys.[30] They reported that the as-cast sample exhibited less resistance toward oxidation compared to the solution heat-treated samples, and the alloy with higher Co concentration showed lower oxidation resistance. But only limited studies consider the effect of the solution heat-treatment and segregation of the elements on the oxidation resistance of the Ni-base SC superalloys. Therefore, it is difficult to determine the lower limit of solution heat-treatment temperature necessary to maintain the level of oxidation resistance which the designed alloy originally has, all while considering the reduction of the process cost.

The objective of this research is to clarify the effect of solution heat-treatment on the oxidation resistance of Ni-base SC superalloy, by comparing the as-cast material and solution heat-treated material. The compositions of the dendrite core and inter-dendrite within the superalloy were analyzed, and the differences in the structures of the oxide layers were evaluated.

II. EXPERIMENTAL PROCEDURES

Single-crystal Ni-base superalloy TMS-238[14] was used for this research. The alloy was cast into the SC alloy by using the directional solidification furnace. High-frequency vacuum induction heating was used to melt the materials and kept at 1600 °C for 15 minutes under 6×10^{-2} Pa. The melt was poured into the mold and withdrawn from the heating chamber to the cooling chamber at 200 mm/h to be unidirectionally solidified into single crystal cylindrical bars, with diameters of 11 mm. The alloy compositions were analyzed using inductively coupled plasma optical emission spectrometer (ICP-OES) for most of the elements except S, which was analyzed using glow discharge mass spectrometry (GD-MS). One sample was not heat-treated, which will be referred to as the as-cast sample. The other sample was heat-treated at 1335 °C for 20 hours, which is known to be enough for the TMS-238 to be homogenized.[11] Aging heat-treatment was not conducted for this research since we are only focusing on the dendritic segregation of elements. Samples for observations and oxidation tests were cut normal to the growth direction, which is [001], from the cylindrical SC bars to be 5 mm in height and 9 mm in diameter. The surfaces and cross-sections of the samples were polished using U.S. Grid #600 SiC abrasive paper and mirror polished.

The samples were observed using electron probe micro analyzer (EPMA, SHIMADZU EPMA1610) with the accelerating voltage at 15 kV, the beam current at 20 nA, and the beam size at 1 μm. The compositions of the dendrite core and inter-dendrite for each alloy were also analyzed using EPMA. Different areas of the dendrite core and inter-dendrite were analyzed five times each, and the average concentrations were obtained. The gradual changes in the compositions of the as-cast sample were also analyzed using EPMA by point analysis, starting from the dendrite core and ending at the center of inter-dendrite, with each point analysis being 5 μm apart.

Cyclic oxidation tests were conducted at 1100 °C for 150 cycles, where each cycle consists of 1 hour of heating at 1100 °C and 1 hour of cooling in air. Separate samples oxidized at 1100 °C for 10 cycles were observed from the top using field emission scanning electron microscopy (FE-SEM, ZEISS GeminiSEM300). Samples were also isothermally oxidized at 1100 °C for 10 minutes, and the cross-section of the oxides scales that had formed in both the dendrite core and inter-dendrite were observed by creating cross-sections using focused ion beam (FIB) milling and observed using scanning electron microscopy and energy-dispersive spectroscopy (SEM-EDS, ZEISS Gemini 2 Crossbeam 550). This is sufficient amount of time for the oxide layer to grow and be intact for observation. The cross-sectional elemental maps of the oxide scales for both samples were obtained using SEM-EDS (ZEISS Gemini 2 Crossbeam 550) as well.

III. RESULTS

Figure 1 shows the back-scattered electron images (BEIs) of both the as-cast and heat-treated samples. The as-cast sample shows clear image of the dendrites, while the dendrites for the heat-treated sample have faded. This indicates that the diffusion of elements occurred, and some of the segregation had cleared. The compositions of the alloy analyzed using ICP-OES and GD-MS, as well as the compositions at the dendrite core and inter-dendrite analyzed using EPMA are shown in Table I. Al, which tends to partition into the liquid phase during solidification, and segregates to the inter-dendrite. On the other hand, Cr, which tends to partition into the solid phase, segregates to the dendrite core. For the as-cast material, there was a clear difference in the composition between the dendrite core and inter-dendrite. For example, the amount of Al was significantly larger at the inter-dendrite. On the other hand, the amount of Cr was larger at the dendrite core. The heat-treated sample had similar compositions at the dendrite core and inter-dendrite, suggesting that the sample had been homogenized successfully.

To understand whether heat-treatment affects the oxidation resistance of the alloy, cyclic oxidation tests were conducted at 1100 °C, and the results are shown in Figure 2. The results for the cyclic oxidation of TMS-238 samples with low S and fully heat-treated by conducting both solution heat-treatment at 1345 °C for 20 hours and aging heat-treatments at 1150 °C for 2 hours, and 870 °C for 20 hours are shown as Reference 31. The referenced results have almost the same

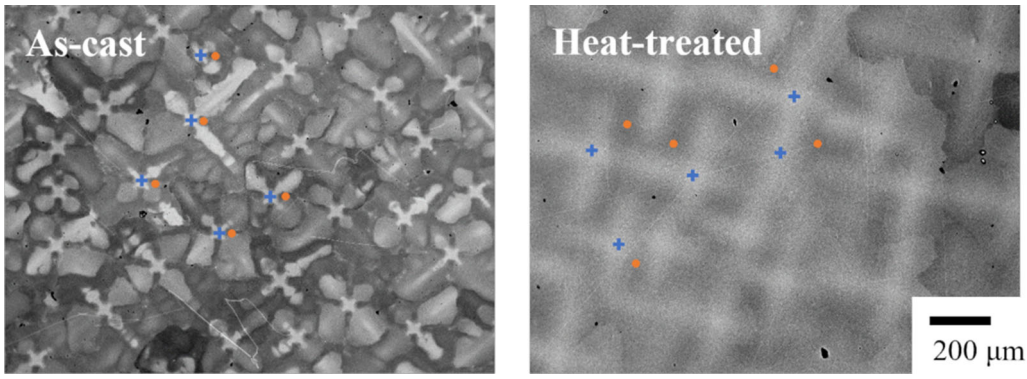

Fig. 1—BEIs of the as-cast and the heat-treated (1335 °C 20 h) TMS-238. The light areas are dendrite cores, while the dark areas are inter-dendrites. The analyzed areas for the chemical compositions shown in Table I are added in the BEIs as blue crosses for the dendrite cores, and orange circles for the inter-dendrites (Color figure online).

Table I. Nominal[14] and Analyzed Compositions of TMS-238 (Ni bal.)

		Compositions										
		Wt Pct									ppm	
Sample/Location		Co	Cr	Mo	W	Al	Ta	Re	Ru	Hf	S	Analysis Method
Nominal[14]		6.5	4.6	1.1	4.0	5.9	7.6	6.5	5.0	0.1	—	
Analyzed		6.3	4.4	1.1	4.0	6.0	7.8	6.3	5.0	0.1	2.4	ICP-OES, (GD-MS for S)
As-Cast	Dendrite Core	6.6	4.6	1.1	5.7	4.8	5.4	11.5	5.3	0.2	—	EPMA
	Inter-dendrite	5.1	2.8	0.7	1.9	7.4	13.2	1.7	4.4	0.2	—	
Heat-Treated	Dendrite Core	6.5	4.5	1.1	4.0	5.7	7.3	7.4	5.0	0.3	—	EPMA
	Inter-dendrite	6.4	4.7	1.1	4.1	5.6	7.9	5.6	5.4	0.1	—	

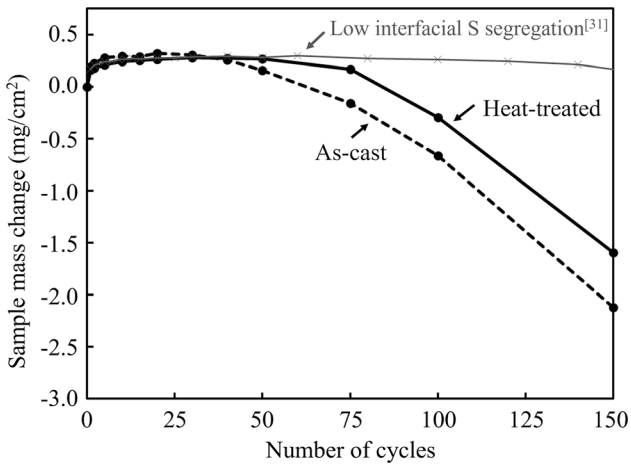

Fig. 2—Sample mass changes of the as-cast and the heat-treated TMS-238 under 1100 °C 1 h cyclic oxidation tests. Results for fully heat-treated (solution and aging) TMS-238 samples with low S segregation level are shown as a Ref. [31].

microstructure for the oxide layer, but the S segregation level has been suppressed, leading to the reduction in spallation of the oxides. The differences in the cyclic oxidation between the heat-treated sample and the referenced results are most likely due to the differences in the S segregation level. The as-cast sample had slightly larger change in mass at the beginning of the cyclic oxidation test. By 75 cycles, there was a clear difference between the two samples, where the heat-treated sample had less changes in mass compared to the as-cast sample.

To observe the difference in the initial oxidation resistance, secondary electron images (SEIs) taken from the top of both samples oxidized at 1100 °C for 10 cycles were observed, as shown in Figure 3(b) for the as-cast sample, and Figure 4(b) for the heat-treated sample. The directions of the observations are shown in the schematic diagrams in Figures 3(a) and 4(a). For the as-cast sample, oxide spallation can be observed around the dendrite core, shown in dotted white lines, and the shape of the dendrites can be seen within the area where the oxides had spalled. On the other hand, the heat-treated sample showed no signs of spallation, and the oxides were intact. Therefore, it has been made clear that without solution heat-treatment, the oxidation resistance of the SC superalloys decreases. To understand if there were any differences in the structures of the oxide layers, samples oxidized at 1100 °C for 10 minutes were also prepared and observed, shown in Figure 3(c) for the as-cast samples, and Figure 4(c) for heat-treated samples. The cross-sections were created using FIB milling and observed using SEM. The locations where the milling and observations were conducted are shown in the schematic diagrams in Figures 3(a) and 4(a). In

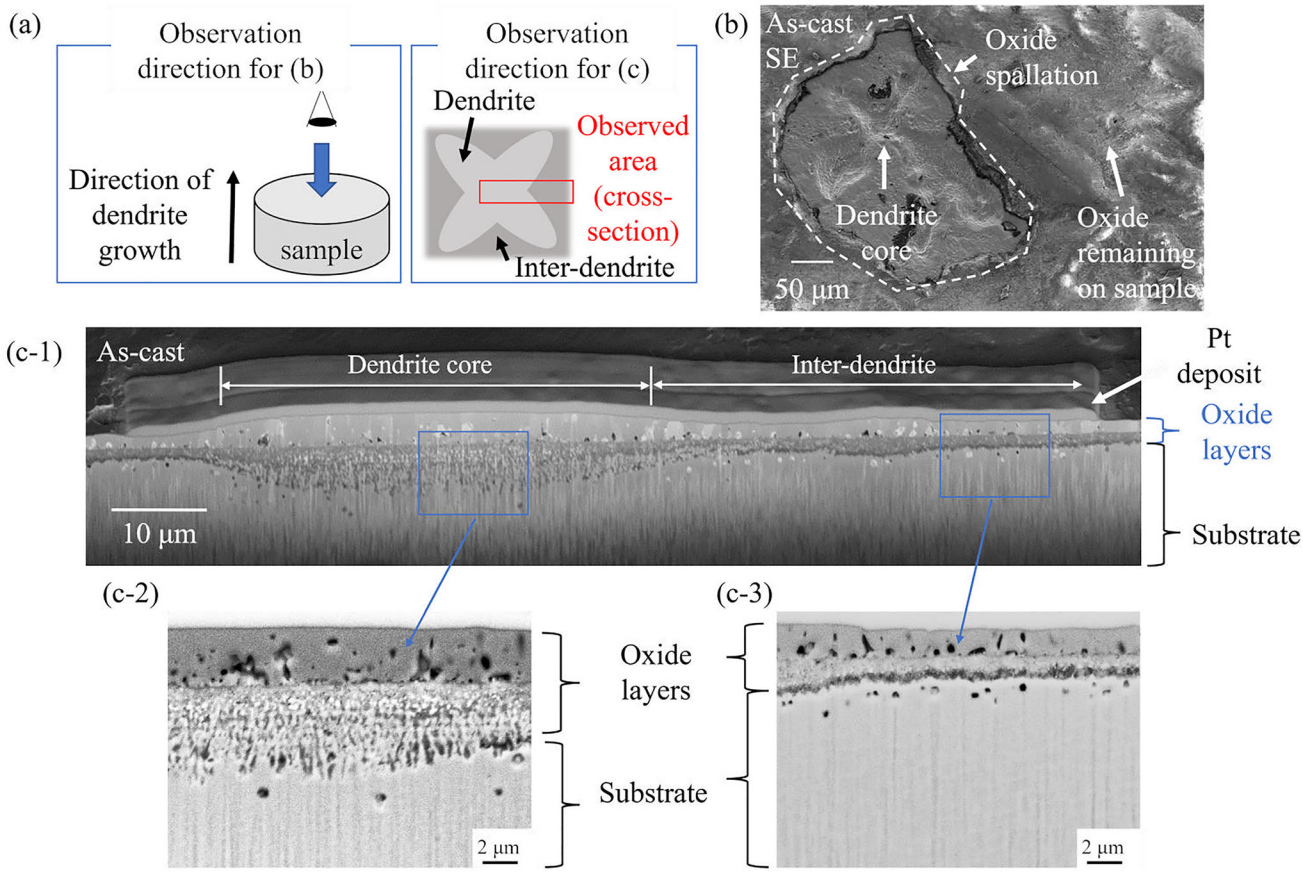

Fig. 3—SEM images of an oxidized as-cast sample. (*a*) Schematic diagrams showing the directions of observations. (*b*) Top view of sample oxidized at 1100 °C for 10 cycles, with the white dotted lines showing the area of oxide spallation. (*c*-1) Cross-sectional BEI of isothermal oxidation test at 1100 °C for 10 min, with the blue rectangles representing where the enlarged images of (*c*-2) the dendrite core and (*c*-3) inter-dendrite were taken (Color figure online).

Figure 3(c-1), which shows the BEI of the cross-section of as-cast sample that had been oxidized, clear differences in the thickness of the oxide scales were observed, depending on the location. In Figure 3(c-2), the dendrite core had thick layers with discontinuous and spinel-like oxides, whereas in Figure 3(c-3), for the inter-dendrite, the layers are continuous and less than half in width. For heat-treated samples, however, continuous oxide layers had formed in both the dendrite core and inter-dendrite. As shown in Figures 4(c-1) and (c-2), the thickness of the oxide layers was roughly even throughout the whole sample.

In order to observe the difference in the compositions of the oxide layers, SEIs and EDS elemental maps of the oxide layers for both as-cast and heat-treated samples oxidized at 1100 °C for 10 minutes were taken, as shown in Figure 5. The oxide scales of the samples oxidized at 1100 °C usually consist of NiO on top, followed by the mixture layer of mainly Cr_2O_3, and the Al_2O_3 on top of the substrate.[17] Therefore, we focused our analyses on the elements known to form the oxide layers: Ni, Al, and Cr. For the as-cast sample, the elemental maps of the oxide scales, taken from the area shown in blue, for the dendrite core are shown in Figure 5(a), and the results for the inter-dendrite are shown in Figure 5(b). For the dendrite core, the oxide layers were mostly Cr_2O_3, and the continuous Al_2O_3 layer could not be observed. For the inter-dendrite, continuous Al_2O_3 layer was observed, and both the Cr_2O_3 layer and NiO layer were half the size of the layers observed in the dendrite core. Similar results were obtained for the heat-treated sample shown in Figure 5(c), where continuous Al_2O_3 layer could be observed in the SEI and EDS mapping for Al.

IV. DISCUSSION

Our finding here clearly shows that rapid oxide growth at dendrite core in the as-cast alloy accelerates the spallation during cyclic oxidation, and the oxide growth rate was slower at the inter-dendrite, where continuous Al_2O_3 layer had formed. Meanwhile, it has been reported that the transition criteria for continuous-to-discontinuous Al_2O_3 could be determined by Gibbs energy of the Al_2O_3 formation.[23,24] To further understand the effect of homogenization on the oxidation resistance, here, we summarized the transition distance of continuous-to-discontinuous Al_2O_3 formation (Figure 6(a)), oxide scale thickness (Figure 6(b)), concentration of alloying elements on sub-surface

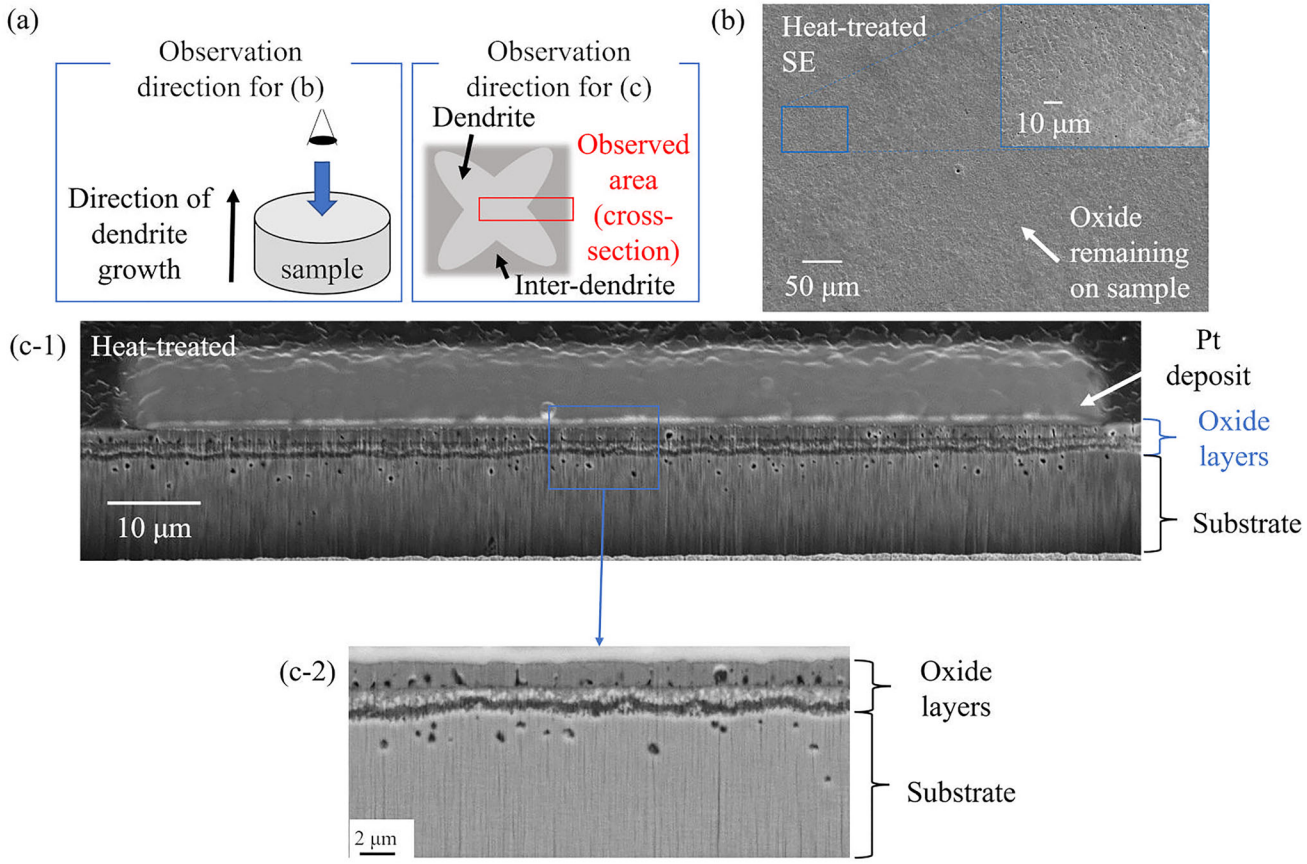

Fig. 4—SEM images of an oxidized heat-treated sample. (*a*) Schematic diagrams showing the directions of observations. (*b*) Top view of sample oxidized at 1100 °C for 10 cycles, and (*c*-1) cross-sectional BEI of isothermal oxidation test at 1100 °C for 10 min, with the blue rectangle representing where the (*c*-2) enlarged image of the interface was taken (Color figure online).

(Figure 6(c)), and calculated Al activity and Gibbs energy of the Al_2O_3 formation (Figure 6(d)), within the dendrite core to inter-dendrite for the as-cast sample oxidized at 1100 °C for 10 minutes. The two vertical dotted lines shown in Figures 6(a) through (d) represent where the continuous Al_2O_3 layer started to form. The red circles in Figure 6(a-1) represent where the point analysis was conducted, and the width of the oxide scales was taken directly above these points.

As SEM images shown in Figure 6(a), the transitions from discontinuous-to-continuous Al_2O_3 formation are found at the distance $D = 21.8$ μm and 59.5 μm, which are shown in white arrows in Figures 6(a-1) and (a-2), respectively. The changes in the total thickness of the oxide scales are shown in Figure 6(b), and the thickness of the layers decreased from the dendrite core to the inter-dendrite. In particular, the thickness of the layers was less than 6.3 μm, shown as a horizontal dotted line in Figure 6(b), within the range of $D = 21.8$ to 59.5 μm where continuous Al_2O_3 layer had formed. This was determined by the merging points of the vertical dotted lines and the line profile. The changes in the concentration for each element measured by EPMA are shown in Figure 6(c), which was made sure that the measurement avoided the Al depletion zone.

The Gibbs energy of the formation of Al_2O_3, $\Delta G_f^{Al_2O_3}$, for multicomponent alloys corresponding to each point in Figure 6(c) can be calculated by following equation, and the results are shown in Figure 6(d):

$$\Delta G_f^{Al_2O_3} = \Delta G_0 + RT\ln\left\{\frac{a_{Al_2O_3}^{2/3}}{a_{Al}^{4/3}\times P_{O_2}}\right\} \quad [1]$$

where ΔG_0 is the standard free energy of Al_2O_3 formation; T is the oxidation test temperature (K); R is the gas constant (= 8.31 J/(mol K)); P_{O_2} is the partial pressure of oxygen, which is 0.021 MPa; and $a_{Al_2O_3}$ is the activity of Al_2O_3 ($a_{Al_2O_3} = 1$ for solid state); a_{Al} is the Al activity in multicomponent compositions. In order to evaluate how the changes in the composition from dendrite core to inter-dendrite affect the tendency of the formation of protective oxide scales, in this study, Al activity was calculated using Thermo-Calc™ (TCNI8: Ni-Alloys v8.0) at 1100 °C, with the compositions shown in Figure 6(c). Although it is difficult to address the effects of each alloying element and their segregation on the oxidation of the alloy, the Al activity calculated in Figure 6(d) incorporates the differences in the compositions, implying the effect on alumina protective layer formation. The absolute value of $\Delta G_f^{Al_2O_3}$ increased at the inter-dendrite, supporting the result that Al_2O_3 tends to form at the inter-dendrite, rather than the dendrite core for the as-cast sample. The merging points of the vertical dotted lines and the line profiles of

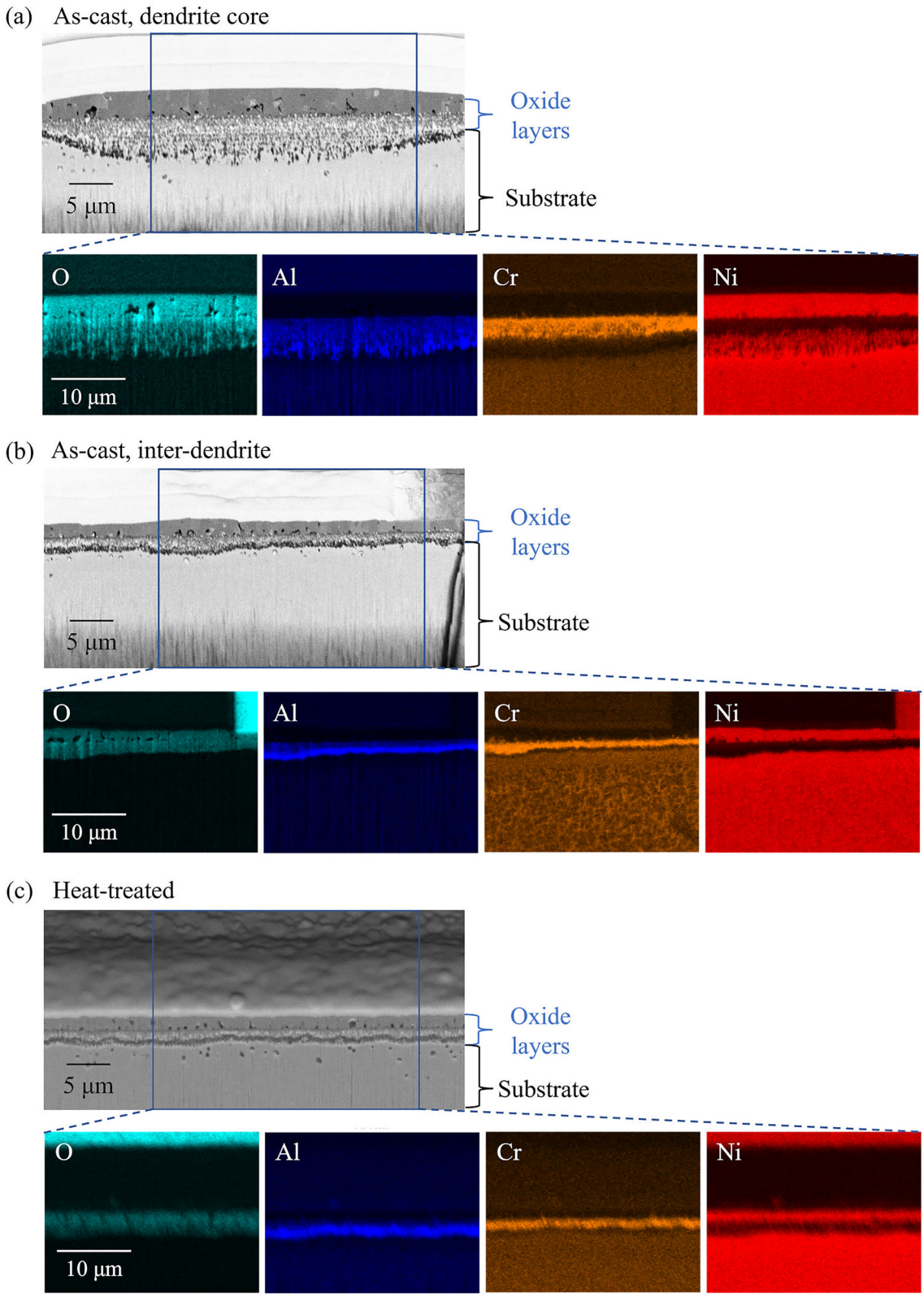

Fig. 5—SEI and EDS elemental maps of O, Al, Cr, and Ni, taken of the cross-section of the as-cast sample at (*a*) dendrite core, (*b*) inter-dendrite, and (*c*) the heat-treated TMS-238. The blue rectangles represent where the EDS analyses were taken. Both samples were oxidized at 1100 °C for 10 min (Color figure online).

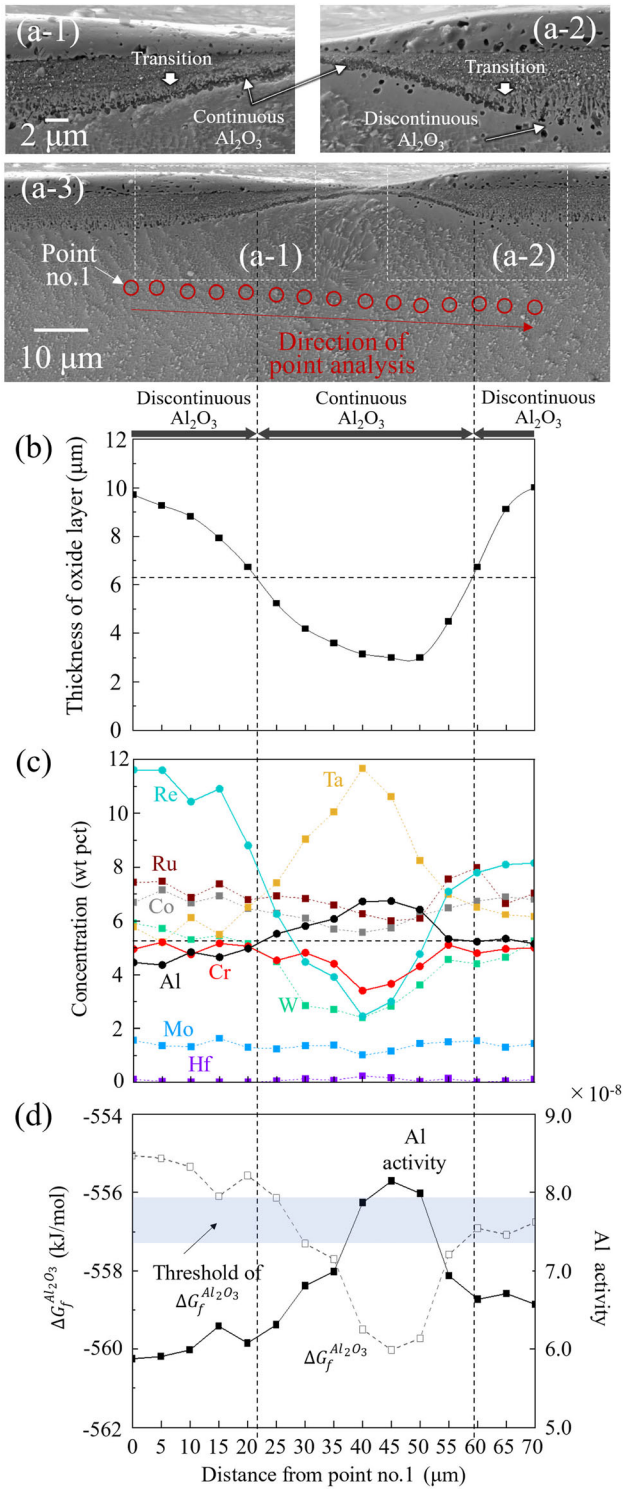

Fig. 6—(*a*-1, *a*-2) Enlarged images and (*a*-3) cross-sectional SEI of the as-cast TMS-238 sample oxidized at 1100 °C for 10 min. Line profiles of (*b*) the changes in the thickness of the oxide layers, and (*c*) changes in the compositions of each element taken using point analysis. (*d*) Line profile showing the changes in calculated Gibbs energy of the formation of Al_2O_3, using the compositions shown in (c), and the activity of Al calculated using Thermo-Calc™ (TCNI8: Ni-Alloys v8.0).

Al concentration and $\Delta G_f^{Al_2O_3}$ drawn represent where the thresholds most likely exist. The horizontal dotted line in Figure 6(c) and the blue area in Figure 6(d) represent the likely range where the threshold of the Al concentration and $\Delta G_f^{Al_2O_3}$ exists for the formation of continuous Al_2O_3 layer. The estimated threshold value of the Al concentration was around 5.2 wt pct and the threshold for $\Delta G_f^{Al_2O_3}$ was -556.6 ± 0.5 kJ/mol.

Next, the adequacy of the borderline concentration of Al and $\Delta G_f^{Al_2O_3}$ necessary to form the continuous Al_2O_3 layer for oxidation at 1100 °C needs to be accessed. Several TMS-238 samples were solution heat-treated at temperatures lower than 1335 °C,[11] and the sample with the Al concentration just above 5 wt pct at the dendrite core was selected. Figure 7 shows SEI of another TMS-238 sample heat-treated at 1305 °C for 20 hours and oxidized at 1100 °C for 10 minutes. The concentration of Al at the dendrite core was around 5.2 wt pct, which corresponds to $\Delta G_f^{Al_2O_3} = 556.1$ kJ/mol and is within the threshold range. The thickness of the continuous Al_2O_3 layer up to 5 μm was observed at both the dendrite core and inter-dendrite for this sample. This result suggests that the samples meant to be oxidized at 1100 °C should be solution heat-treated so that the Al concentration in the dendrite core becomes higher than 5.2 wt pct. Several research also support this threshold value. For Ni-Al binary alloys, the relation between the Al concentration and the parabolic growth rate of the oxides for temperatures between 900 °C and 1200 °C has been previously reported,[32,33] and at 1100 °C, the first drop in the parabolic growth rate of oxides was around 5 wt pct Al as well. The transition to the formation of the stable α-Al_2O_3 layer is known to result in a decrease in scale growth, and only α-Al_2O_3 layers form for 1100 °C.[17,34] Smialek *et al.* also reported that Ni-base superalloys containing more than 5 wt pct Al and up to 6 wt pct Ta showed superior oxidation resistance.[25] Although it is important to note that elements such as Mo, which is known to deteriorate the oxidation resistance of Ni-base superalloys,[25,27] have not changed drastically for this research, elements such as these may affect the borderline Al concentration and $\Delta G_f^{Al_2O_3}$. But can be said that for this temperature and this alloy, the borderline Al concentration and $\Delta G_f^{Al_2O_3}$ found in this study are most likely reasonable.

V. CONCLUSION

To conclude, the following points have been made clear about the effect of solution heat-treatment on the oxidation resistance of Ni-base SC superalloy, TMS-238.

1. Solution heat-treatment at 1335 °C for 20 hours improved the oxidation resistance compared to the as-cast sample, and clear differences in the structure and composition of the oxide layers were observed.

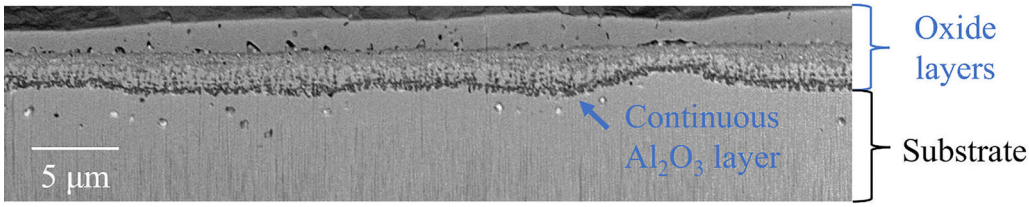

Fig. 7—Cross-sectional SEI of TMS-238 solution heat-treated at 1305 °C for 20 h and oxidized at 1100 °C for 10 min.

The as-cast sample had discontinuous Al_2O_3 formation at the dendrite core, where oxide spallation was mainly observed during the cyclic oxidation tests. The heat-treated sample, however, had continuous Al_2O_3 formation at both the dendrite core and inter-dendrite, clearly suggesting the need to consider the effect of heat-treatment on the oxidation resistance of alloys.

2. For the oxidation of TMS-238 at 1100 °C, continuous Al_2O_3 layer had formed once the Al concentration was higher than 5.2 wt pct, and $\Delta G_f^{Al_2O_3}$ was larger negative than -556.6 ± 0.5 kJ/mol. Continuous Al_2O_3 layer was also observed in an alloy with 5.2 wt pct Al and $\Delta G_f^{Al_2O_3} = -556.1$ kJ/mol in the dendrite core, but with lower solution heat-treatment temperature at 1305 °C for 20 hours. For this alloy, conducting the solution heat-treatment so that the Al concentration and $\Delta G_f^{Al_2O_3}$ for both the dendrite core and the inter-dendrite become higher than the threshold values will most likely be enough for the formation of protective Al_2O_3 scale, thus improving the oxidation resistance.

ACKNOWLEDGMENTS

This paper is based on results obtained from a project, JPNP21007, commissioned by the New Energy and Industrial Technology Development Organization (NEDO). This research was partially supported by the Council of Science, Technology and Innovation (CSTI), Cross-ministerial Strategic Innovation Program (SIP), "Materials integration for revolutionary design system of structural materials" (Funding agency: JST). This research was also supported by Grant-in-Aid for JSPS Fellows Grant Number 23KJ2024. The authors would like to express our gratitude to Dr. Makoto Osawa for the helpful discussions. We also would like to thank Ms. Kyoko Suzuki and Dr. Jun Uzuhashi for the support of microstructural investigation, Mr. Takuma Kohata for the SEM observations, and Mr. Yuji Takata for the preparation of the single-crystal alloys.

CONFLICT OF INTEREST

On behalf of all authors, the corresponding author states that there is no conflict of interest.

OPEN ACCESS

REFERENCES

1. H. Harada, T. Yokokawa, K. Kawagishi, T. Kobayashi, Y. Koizumi, M. Sakamoto, and M. Yuyama: *J. Gas Turbine Soc. Jpn.*, 2015, vol. 43, pp. 349–56.
2. R. Watanabe and T. Kuno: *Tetsu-to-Hagané*, 1975, vol. 61, pp. 126–46.
3. H. Harada and M. Yamazaki: *Tetsu-to-Hagané*, 1979, vol. 65, pp. 337–46.
4. T. Yokokawa, H. Harada, Y. Mori, K. Kawagishi, Y. Koizumi, T. Kobayashi, M. Yuyama, and S. Suzuki: *Superalloys*, 2016, vol. 2016, pp. 123–30.
5. T. Yokokawa, H. Harada, K. Kawagishi, T. Kobayashi, M. Yuyama, and Y. Takata: *Superalloys 2020,* 2021, pp. 122–30.
6. K. Harris, G.L. Erickson, and R.E. Schwer: *Superalloys*, 1984, vol. 1984, pp. 221–30.
7. T. Ohno, R. Watanabe, and A. Yoshinari: *Tetsu-to-Hagané*, 1989, vol. 75, pp. 112–19.
8. A. Yoshinari: *J. JFS*, 2001, vol. 73, pp. 834–39.
9. Y. Koizumi, T. Kobayashi, T. Yokokawa, M. Osawa, H. Harada, T. Hino, and Y. Yoshioka: *J. Jpn. Inst. Met.*, 2003, vol. 67, pp. 205–08.
10. T. Takeshita, Y. Murata, N. Miura, Y. Kondo, Y. Tsukada, and T. Koyama: *J. Jpn. Inst. Met.*, 2015, vol. 79, pp. 203–09.
11. T. Yokokawa, T. Osada, C. Tabata, T. Kohata, Y. Takata, M. Yuyama and K. Kawagishi: *J. Japan Inst. Met. Mater.*, 2023, vol. 87, pp. 288–97.
12. N. D'Souza, D. Welton, G.D. West, I.M. Edmonds, and H. Wang: *Metall. Mater. Trans. A*, 2014, vol. 45A, pp. 5968–81.
13. J. Wahl and K. Harris: *Superalloys*, 2016, vol. 2016, pp. 25–33.
14. K. Kawagishi, A.C. Yeh, T. Yokokawa, T. Kobayashi, Y. Koizumi, and H. Harada: *Superalloys 2012*, 2012, pp. 189–95.
15. K. Nii: *Corros. Eng.*, 1977, vol. 26, pp. 389–400.
16. K. Nii: *Zairyo-to-Kankyo*, 2011, vol. 60, pp. 386–90.
17. N. Birks, G.H. Meier, and F.S. Petit: *Introduction to the High-Temperature Oxidation of Metals*, 2nd ed. Cambridge University Press, New York, 2006, pp. 101–62.

18. K. Kawagishi, A. Sato, T. Kobayashi, and H. Harada: *J. Jpn. Inst. Met. Mater.*, 2005, vol. 69, pp. 249–52.
19. K. Kawagishi, A. Sato, T. Kobayashi, and H. Harada: *J. Jpn. Inst. Met. Mater.*, 2006, vol. 70, pp. 686–89.
20. L. Huang, X. Sun, H. Guan, and Z. Hu: *Oxid. Met.*, 2006, vol. 65(3–4), pp. 207–22.
21. M.H. Li, X.F. Sun, T. Jin, H.R. Guan, and Z.Q. Hu: *Oxid. Met.*, 2003, vol. 60(1–2), pp. 195–210.
22. A.S. Suzuki, K. Kawagishi, T. Yokokawa, T. Kobayashi, and H. Harada: *Superalloys 2012*, 2012, pp. 321–29.
23. A. Sato, Y.L. Chiu, and R.C. Reed: *Acta Mater.*, 2011, vol. 59, pp. 225–40.
24. A. Sato, J.J. Moverare, M. Hasselqvist, and R.C. Reed: *Adv. Mater. Res.*, 2011, vol. 278, pp. 174–79.
25. J.L. Smialek and P.J. Bonacuse: *Mater. High Temp.*, 2016, vol. 33, pp. 489–500.
26. S. Gao, B. He, L. Zhou, and J. Hou: *Corr. Sci.*, 2020, vol. 170, 108682.
27. L. Qin, Y. Pei, S. Li, X. Zhao, S. Gong, and H. Xu: *Corr. Sci.*, 2017, vol. 129, pp. 192–204.
28. C.S. Giggins and F.S. Pettit: *J. Electrochem. Soc.*, 1971, vol. 118, pp. 1782–90.
29. G. Luo, M. Cheng, L. Zhao, Y. Tang, J. Yao, H. Cui, and L. Song: *Corr. Sci.*, 2021, vol. 179, 109144.
30. A.S. Hagen, M. Weiser, B. Abu-Khousa, and S. Virtanen: *Metall. Mater. Trans. A*, 2022, vol. 53A, pp. 1552–71.
31. C. Tabata, K. Kawagishi, J. Uzuhashi, T. Ohkubo, K. Hono, T. Yokokawa, H. Harada, and S. Suzuki: *Scr. Mater.*, 2021, vol. 194, 113616.
32. C.T. Sims, N.S. Stoloff, and W.C. Hagel: *Superalloys II High-Temperature Materials for Aerospace and Industrial Power*, Wiley, New York, 1987, pp. 302–11.
33. F.S. Pettit: *Trans. TMS-AIME*, 1967, vol. 239, pp. 1296–1305.
34. J. Doychak: *Intermetallic Compounds*, eds. J. H. Westbrook, R.L. Fleischer, Wiley, New York, 1994, p. 977.